Extension of the N=40 Island of Inversion towards N=50: Spectroscopy of ^{66}Cr, ^{70,72}Fe

C. Santamaria,[1,2] C. Louchart,[3] A. Obertelli,[1,2] V. Werner,[3,4] P. Doornenbal,[2] F. Nowacki,[5] G. Authelet,[1] H. Baba,[2] D. Calvet,[1] F. Château,[1] A. Corsi,[1] A. Delbart,[1] J.-M. Gheller,[1] A. Gillibert,[1] T. Isobe,[2] V. Lapoux,[1] M. Matsushita,[6] S. Momiyama,[2,7] T. Motobayashi,[2] M. Niikura,[7] H. Otsu,[2] C. Péron,[1] A. Peyaud,[1] E.C. Pollacco,[1] J.-Y. Roussé,[1] H. Sakurai,[2,7] M. Sasano,[2] Y. Shiga,[2,8] S. Takeuchi,[2] R. Taniuchi,[2,7] T. Uesaka,[2] H. Wang,[2] K. Yoneda,[2] F. Browne,[9] L.X. Chung,[10] Zs. Dombradi,[11] S. Franchoo,[12] F. Giacoppo,[13] A. Gottardo,[12] K. Hadynska-Klek,[13] Z. Korkulu,[11] S. Koyama,[2,7] Y. Kubota,[2,6] J. Lee,[14] M. Lettmann,[3] R. Lozeva,[5] K. Matsui,[2,7] T. Miyazaki,[2,7] S. Nishimura,[2] L. Olivier,[12] S. Ota,[6] Z. Patel,[15] N. Pietralla,[3] E. Sahin,[13] C. Shand,[15] P.-A. Söderström,[2] I. Stefan,[12] D. Steppenbeck,[6] T. Sumikama,[16] D. Suzuki,[12] Zs. Vajta,[11] J. Wu,[2,17] and Z. Xu[14]

[1] *CEA, Centre de Saclay, IRFU, F-91191 Gif-sur-Yvette, France*
[2] *RIKEN Nishina Center, 2-1 Hirosawa, Wako, Saitama 351-0198, Japan*
[3] *Institut für Kernphysik, Technische Universität Darmstadt, 64289 Darmstadt, Germany*
[4] *WNSL, Yale University, P.O. Box 208120, New Haven, CT06520, USA*
[5] *IPHC, CNRS/IN2P3, Université de Strasbourg, F-67037 Strasbourg, France*
[6] *Center for Nuclear Study, University of Tokyo, RIKEN campus, Wako, Saitama 351-0198, Japan*
[7] *Department of Physics, University of Tokyo, 7-3-1 Hongo, Bunkyo, Tokyo 113-0033, Japan*
[8] *Department of Physics, Rikkyo University, 3-34-1 Nishi-Ikebukuro, Toshima, Tokyo 172-8501, Japan*
[9] *School of Computing Engineering and Mathematics, University of Brighton, Brighton BN2 4GJ, United Kingdom*
[10] *Institute for Nuclear Science & Technology, VAEI, 179 Hoang Quoc Viet, Cau Giay, Hanoi, Vietnam*
[11] *MTA Atomki, P.O. Box 51, Debrecen H-4001, Hungary*
[12] *Institut de Physique Nucléaire Orsay, IN2P3-CNRS, 91406 Orsay Cedex, France*
[13] *Department of Physics, University of Oslo, N-0316 Oslo, Norway*
[14] *Department of Physics, The University of Hong Kong, Pokfulam, Hong Kong*
[15] *Department of Physics, University of Surrey, Guildford GU2 7XH, United Kingdom*
[16] *Department of Physics, Tohoku University, Sendai 980-8578, Japan*
[17] *State Key Laboratory of Nuclear Physics and Technology, Peking University, Beijing 100871, P.R. China*

We report on the measurement of the first 2^+ and 4^+ states of ^{66}Cr and ^{70,72}Fe via in-beam γ-ray spectroscopy. The nuclei of interest were produced by $(p, 2p)$ reactions at incident energies of 260 MeV/nucleon. The experiment was performed at the Radioactive Isotope Beam Factory, RIKEN using the DALI2 γ-ray detector array and the novel MINOS device, a thick liquid hydrogen target combined with a vertex tracker. A low-energy plateau of 2_1^+ and 4_1^+ energies as a function of neutron number was observed for N$\geq$38 and N$\geq$40 for even-even Cr and Fe isotopes, respectively. State-of-the-art shell model calculations with a modified LNPS interaction in the $pfg_{9/2}d_{5/2}$ valence space reproduce the observations. Interpretation within the shell model shows an extension of the Island of Inversion at N=40 for more neutron-rich isotopes towards N=50.

PACS numbers: 21.10.Re, 21.60.Cs

Atomic nuclei are the place of a complex interplay between single-particle configurations and correlations which strongly determine their quantum coherent wave-functions. All over the nuclear chart, the so-called *magic* numbers of nucleons define boundaries of large areas of deformation. This picture, mainly established for stable nuclei and neighbors, is re-examined at the light of new available nuclei with an unbalanced proton-to-neutron ratio, with the underlying question of the persistence or evolution of magic numbers [1, 2]. Specific terms of the nuclear interaction can induce the formation of shell gaps or the lowering of relative orbital energies which, combined with correlations, sometimes lead to energetically favored intruder states as the ground state configuration [3–8]. Regions where two-particle two-hole ($2p2h$) configurations are favored over normally-filled orbitals by quadrupole correlations have been termed as *Islands of Inversion* (IoI) [9–11]. The N=20 IoI in the vicinity of ^{32}Mg has provided unique information on shell evolution [12]. This IoI does not show any decrease in collectivity for Mg isotopes at $N > 24$ and merges with the N=28 deformation region [8, 13]. For Fe and Cr isotopes at N=40, a similar IoI has been claimed [14] while ^{68}Ni shows a marked pf neutron shell closure with a high excitation energy of the 2_1^+ state [15] and small B(E2; $0_1^+ \rightarrow 2_1^+$) (B(E2)$\uparrow$) value [16]. On the other hand, mass measurements show that the N=40 gap is weak for ^{68}Ni [17, 18] and it has been proposed that the low B(E2)$\uparrow$ value in ^{68}Ni may not be due to a N=40 shell closure but might come from a neutron-dominated excitation [19]. The removal of only two protons from the $f_{7/2}$ orbital has a drastic effect on the collectivity in Fe isotopes and changes the energy of the 2_1^+ state from 2033 keV in ^{68}Ni to 573 keV and 517 keV in ^{66}Fe and ^{68}Fe, respectively [20, 21]. A similar behavior is observed in the Cr isotopes, where

the 2_1^+ energies decrease gradually beyond N=32 [22, 23] with the lowest 2_1^+ energy measured in this mass region at 420(7) keV for ^{64}Cr [24]. This sudden onset of deformation along the Fe and Cr chains has also been inferred from B(E2)↑ systematics [14, 25, 26]. Those first observables demonstrate an increase of collectivity for both Cr and Fe isotopes as a function of neutron number beyond N=38, which is also supported by mass measurements [27]. This is well reproduced within the shell model with a $pfg_{9/2}d_{5/2}$ valence space for neutrons and pf valence space for protons outside a ^{48}Ca core [28]. Significant neutron excitations above the $1g_{9/2}$ orbital to its quadrupole partner $2d_{5/2}$ have been shown to play a major role in this effect. Beyond-mean field calculations based on a collective Hamiltonian lead to similar predictions [29, 30]. The scarce experimental data available on Cr and Fe isotopes beyond N=40 indicate that no maximum of collectivity has been reached. Whether the structural evolution of the heavier isotopes mimics the merging found for Mg isotopes depends on the persistence of the N=50 shell closure below ^{78}Ni [31]. In this Letter, we present the first spectroscopy of ^{66}Cr and ^{70,72}Fe and characterize the evolution of collectivity inside the N=40 IoI towards N=50.

The experiment was performed at the Radioactive Isotope Beam Factory (RIBF), operated jointly by the RIKEN Nishina Center and the Center for Nuclear Study of the University of Tokyo. A ^{238}U beam was accelerated to 345 MeV/nucleon and impinged on a 3-mm thick ^{9}Be primary target at the entrance of the BigRIPS separator [32] with a mean intensity of 12 pnA. The secondary beam was selected by the $B\rho$-ΔE-$B\rho$ method with 8-mm and 2-mm thick aluminum wedges at two dispersive planes. Two beam settings were tuned for ^{67}Mn and ^{71,73}Co, respectively. Fully-stripped secondary ions were identified on an event-by-event basis. The particle identification of the incoming cocktail beam at the entrance of the secondary target and the identification of secondary residues were performed from Bρ reconstruction, time of flight, and ionization-chamber energy loss measurements in the BigRIPS and ZeroDegree (ZDS) spectrometers [33]. The incident energies at the entrance (exit) of the secondary target were ∼260 (∼200) MeV/nucleon for ^{67}Mn and ^{71,73}Co. Their intensities were measured to be 12 s^{-1}, 45 s^{-1}, and 6 s^{-1}, respectively. The total beam intensity on target for each of the two settings was about 6 kHz. This experiment was the first performed with the SEASTAR [34] setup composed of the DALI2 high-efficiency gamma spectrometer [35] and the new MINOS device integrating a liquid hydrogen target and a Time Projection Chamber (TPC) as a vertex tracker [36] (see Fig. 1). The SEASTAR setup ensured a gain in luminosity of 3.5 compared to the use of a solid Be target with the same energy loss. The vertex tracker

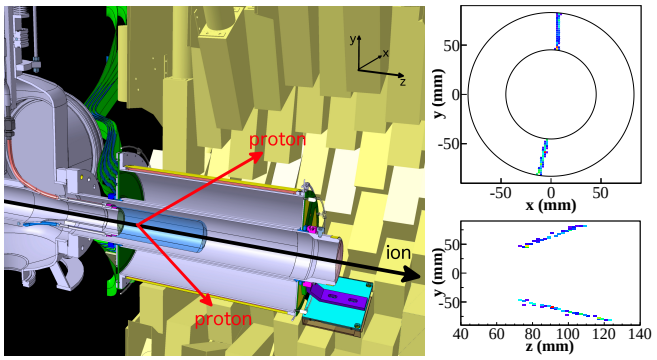

FIG. 1: (Color online) (Left) Drawing of the setup. The MINOS TPC (grey) and target (blue) are surrounded by the DALI2 array (yellow) in a compact geometry. (Right) A typical ^{67}Mn$(p,2p)^{66}$Cr event measured with MINOS. The induced charges produced by ionization electrons were collected on the Micromegas detector in the xy transverse plane (top) whereas the directions of the tracks along the z axis were obtained from the drift time (bottom).

(i) improved the Doppler correction for the decay of short lived states by minimizing target effects and (ii) selected only the reaction events that occurred inside the target. The target cell was 102(1) mm long and filled with pure liquid hydrogen at 20 K, leading to an effective target thickness of 735(8) mg/cm^2. The entrance and exit target windows added up to 275 μm of Mylar. Beam particles were tracked with two position-sensitive parallel-plate avalanche counters [37] upstream of the target. Secondary residues were mostly produced from hydrogen-induced $(p,2p)$ knockout reactions. MINOS measured the emitted proton trajectories, from which the vertex was reconstructed. As an example, a typical $(p,2p)$ event is shown in the right panel of Fig. 1. Events with one or two protons were detected and reconstructed with a 95% efficiency and a vertex position resolution along the beam axis better than 5 mm Full Width at Half Maximum (FWHM) [38]. The 300-mm long cylindrical TPC was flushed with a gas mixture of Ar (82%), isoC$_4$H$_{10}$(3%) and CF$_4$ (15%) at room temperature and atmospheric pressure. The electron drift velocity was measured to be 4.5 cm/μs, for a 180 V/cm homogeneous electrical potential, in agreement with simulations. Ionization electrons from tracks of charged particles through the TPC volume were amplified by a bulk Micromegas [39] plane composed of 3604 constant-area pads divided into 18 rings. The longitudinal direction of the tracks was determined from the electron drift time measured with new custom-made readout electronics [40]. This work was the first sizable experiment using AGET chips [41], a key component to handle a trigger of several hundred Hz. The DALI2 array was composed of 186 NaI scintillator detectors with an energy threshold of ∼200 keV and covering angles from 7 to 115 degrees

(integrated along the target length) relative to the beam axis in a close geometry around the MINOS device as illustrated in Fig. 1. Energy calibrations were performed with ^{88}Y, ^{137}Cs, and ^{60}Co gamma sources giving a 2.9 % sigma energy resolution for a 1333 keV γ-ray transition. The setup was estimated to have a 32 % (20 %) full-energy photopeak detection efficiency for a 500 keV (1 MeV) transition emitted in-flight at 250 MeV/nucleon without addback. The Doppler correction of γ-ray transitions emitted in-flight was performed by taking into account the reaction vertex and the projectile velocity, reconstructed from MINOS. The procedure was validated on known short-lived cases. Addback was performed for γ-ray energies greater than 200 keV when the center of hit detectors were less than 15 cm apart.

The Doppler-corrected γ-ray spectra for ^{66}Cr, and ^{70,72}Fe are shown in Fig. 2. Two transitions are visible for all three nuclei. In the case of ^{66}Cr the transition energies were found at 386(10) keV and 683(9) keV, for ^{70}Fe at 480(13) keV and 866(10) keV, and for ^{72}Fe at 520(16) keV and 814(12) keV. Due to limited statistics, no other transition was observed. Gamma-gamma coincidences are illustrated in the insets of Fig. 2. From relative intensities and from the systematics along the Fe and Cr chains, the first two γ-ray lines were assigned to the $2_1^+ \rightarrow 0_1^+$ and $4_1^+ \rightarrow 2_1^+$ transitions. Note that one proton knockout reactions from the fp shells can naturally lead to J=4 states, and that the relative intensities of the first 2^+ and 4^+ states populated from $(p,2p)$ and $(p,3p)$ are similar for the three studied nuclei, as well as for the cases of ^{68}Fe and ^{74}Ni for which the $4^+ \rightarrow 2^+$ transitions are unambiguously assigned in the literature. Absolute cross sections will be discussed elsewhere. These energy values were obtained from a fit containing the simulated response of DALI2 [42] and background consisting of two exponentials. The experimental intrinsic resolution of each crystal was considered in the simulations. The summed simulated spectra are shown with the experimental data in Fig. 2, as well as the simulated responses for individual transitions. The half-lives of the γ-ray emitting states affect the peak positions after applying the Doppler correction. In the case of a 386/480/520 keV transition, simulations yield an offset of 8/11/13 keV for a 50 ps half-life. In the simulations, we considered the half-life of 2_1^+ states to be 50 ps for ^{66}Cr and ^{70,72}Fe, in agreement with known half-lives in this mass region and with the measured widths of the transitions. The uncertainty on this half-life was considered of $\pm$50 ps for all the nuclei and was included in the energy uncertainties for the $2_1^+ \rightarrow 0_1^+$ transition. 4_1^+ states were considered short-lived ($\tau_{1/2} < 10$ ps). These half-life uncertainties, dominating the 2_1^+ energy ones, were added quadratically to statistical and energy calibration (5 keV) uncertainties.

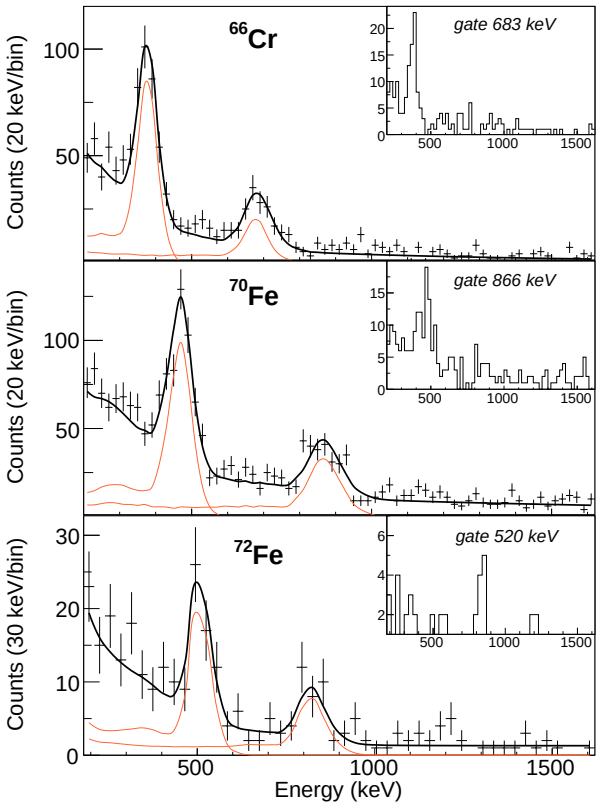

FIG. 2: (Color online) Doppler-corrected γ-ray spectra of ^{66}Cr, ^{70}Fe, and ^{72}Fe, populated from $(p,2p)$ and $(p,3p)$ reactions: data, simulated responses for all transitions (orange), and sum of the simulated transitions with a two-exponential background (black). Multiplicities below five are shown. (Insets) Gamma-gamma coincidence spectra.

The systematics of 2_1^+ energies and the ratio $R_{4/2}$=E(4_1^+)/E(2_1^+) of even-even nuclei belong to the first observables that can be measured with rare isotopes and provide information on their collectivity. The evolution of 2_1^+ and 4_1^+ states is presented in Fig. 3. At first glance, the measured 2_1^+, 4_1^+ energies reveal a rather flat behavior from N=38 to N=42 for Cr isotopes and from N=40 to N=46 for Fe isotopes, suggesting that the bulk deformation properties of these isotopes do not evolve much beyond N=40 and that ^{66}Cr and ^{70,72}Fe stay within the IoI. In a simple collective model, one expects the maximum of collectivity along an isotopic chain to lead to a minimum 2_1^+ energy and a $R_{4/2}$ ratio close to 3.3 in case of pure rotational states. In this framework, the picture obtained from this measurement is consistent. The Cr chain shows increasing collectivity towards ^{66}Cr with the lowest 2_1^+ energy measured in the region of ^{66}Cr while the $R_{4/2}$ ratio increases. The same picture is true for Fe isotopes from N=40, while a change is observed at N=46: both the 2_1^+ energy and the $R_{4/2}$ ratio consistently indicate a lessening of the collectivity from N=44. This change, occurring at

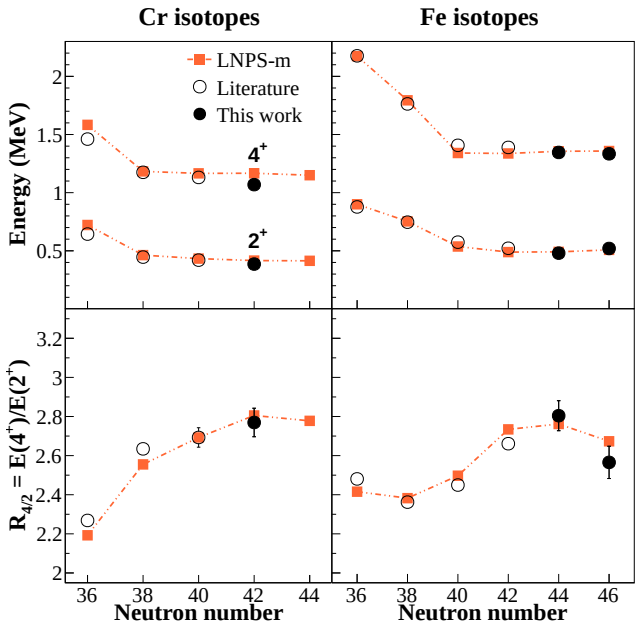

FIG. 3: (Color online) Systematics of $E(2_1^+)$ and $E(4_1^+)$ energies and $R_{4/2}$=$E(4_1^+)$ /$E(2_1^+)$ for Cr and Fe isotopes. Experimental energies from Refs. [21, 24, 43] and from the present work are compared to large-scale shell model calculations. Most error bars are too small to be seen.

the $g_{9/2}$ *mid-shell*, is observed for the first time in the N=40 Island of Inversion. Although this behavior would be typical for an isolated $g_{9/2}$ single shell, the actual situation turns out to be more subtle.

To further quantify the collectivity in neutron-rich Cr and Fe isotopes beyond N=40, shell model calculations were carried out in the valence space that successfully described the new IoI at N=40 [28]. This valence space was composed of the *pf* proton orbitals and $p_{1/2}$, $f_{5/2}$, $g_{9/2}$, and $d_{5/2}$ neutron orbitals. The effective Hamiltonian used in this work, called LNPS-m, was based on the LNPS Hamiltonian from Ref. [28]. Minor modifications to the LNPS interaction were applied on the monopole and pairing parts of the effective Hamiltonian to describe a broader region [44–46]. In addition, LNPS calculations underpredict the 2_1^+ excitation energies of the most neutron rich Cr and Fe isotopes, which was interpreted as missing intruder configurations in their ground state. This mechanism is cured and validated by introducing 150 keV additional *gd-gd* monopole strength in the present LNPS-m interaction. The physics at N=40 remains unchanged with respect to the LNPS Hamiltonian (see for example occupancies and wavefunction decomposition for ^{64}Cr in Table I and Table II of Ref. [28]) but the root mean square for all the states in Fig. 3 amounts to 49 keV with the present LNPS-m Hamiltonian against 89 keV with the original LNPS. More detailed results with the LNPS-m interaction will be discussed elsewhere. The need and

TABLE I: Quadrupole deformation properties of Cr and Fe isotopes. Energies are in MeV, $B(E2)\downarrow$ in e^2 fm^4, and Q in e fm^2. Experimental energies are the same as Fig. 3.

	^{62}Cr	^{64}Cr	^{66}Cr	^{68}Cr	^{66}Fe	^{68}Fe	^{70}Fe	^{72}Fe
$E^*(2_1^+)$ exp.	0.44	0.42	0.39	-	0.57	0.52	0.48	0.52
$E^*(2_1^+)$ theo.	0.46	0.43	0.42	0.41	0.54	0.49	0.49	0.51
Q_{spec}	-38	-38	-39	-38	-37	-40	-39	-33
B(E2)$\downarrow$ th.	378	388	389	367	372	400	382	279
Q_{int} from Q_{spec}	135	136	137	132	131	140	135	116
Q_{int} from B(E2)	138	140	140	136	137	142	139	118
$<\beta>$	0.33	0.33	0.32	0.30	0.29	0.30	0.28	0.24
$E^*(4_1^+)$ exp.	1.17	1.13	1.07	-	1.41	1.39	1.35	1.33
$E^*(4_1^+)$ theo.	1.18	1.13	1.06	1.15	1.34	1.34	1.36	1.36
Q_{spec}	-49	-49	-46	-47	-47	-51	-48	-40
B(E2)$\downarrow$ th.	562	534	562	530	553	608	574	377
Q_{int} from Q_{spec}	135	134	134	130	129	141	132	111
Q_{int} from B(E2)	141	140	141	137	139	146	142	115
$<\beta>$	0.34	0.33	0.32	0.31	0.29	0.30	0.29	0.23

impact of this extra term are discussed hereafter. The overall 2_1^+, 4_1^+ systematics and observed plateaus are reproduced by the calculations. The collectivity of these nuclei can be estimated using the rotational limit where a connection between the laboratory and intrinsic frames is established using relations (1) and (2) of Ref. [28]. The quadrupole properties of these nuclei are summarized in Table I. The calculated B(E2)$\downarrow$ values, quadrupole moments and deformations are consistent with a first-order description of the studied isotopes as prolate deformed rotational nuclei. An interesting feature for the studied nuclei is that the intrinsic wave functions for the ground, 2^+ and 4^+ states for all studied nuclei are shown to be similar with a relative variation of neutron occupancy $n^\nu(g_{9/2}+d_{5/2})$ of less than 3 % along the band states. In the Cr chain, the calculations show that the deformation is nearly constant with a maximum achieved at N=40 where the quadrupole collectivity translates into the development of an intrinsic shape of deformation $\beta \sim 0.33$. This feature is reflected by almost constant 2_1^+ and 4_1^+ excitation energies. Nevertheless, inspection of the wave function content in Table II shows varying particle-hole excitations as a function of the neutron number, and a maximum at N=40 with sizable $6p6h$ excitations admixtures. Similar conclusions can be drawn for Fe isotopes and details on their wave functions can be obtained from calculations performed with the original LNPS interaction in Ref. [14, 28]. To understand the flat behavior of 2_1^+ excitation energies in the Cr and Fe chains, we extracted the pairing expectation value of the multipole Hamiltonian for both the ground and first excited states. Our study indicates a delicate interplay between quadrupole and pairing correlations. For example ^{66}Cr and ^{70}Fe show

TABLE II: Occupation number n^{ν} of neutron intruder orbitals from the shell-model calculations (SM) of this work compared to the independent particle model (IPM). The percentage of particle-hole excitations across the N=40 gap in the ground state of Cr isotopes is also given. The last column features the pairing correlations energy differences $\Delta E^{*}_{Pairing}$ (in MeV) evaluated between the ground state and the 2^{+}_{1} state.

Nucleus	$n^{\nu}(g_{9/2}+d_{5/2})$		$0p0h$	$2p2h$	$4p4h$	$6p6h$	$\Delta E^{*}_{Pairing}$
	IPM	SM					
^{60}Cr	0	1.8	14	75	7	0	1.84
^{62}Cr	0	3.5	1	25	71	3	1.49
^{64}Cr	0	4.3	0	8	71	20	1.25
^{66}Cr	2	5.2	0	40	56	3	1.13
^{68}Cr	4	6.0	6	79	11	0	1.24

the smallest 2^{+}_{1} excitation energy of their respective isotopic chain as a consequence of a smaller pairing correlations difference between the ground-state and the 2^{+}_{1}. Our work also demonstrates that intruder states are very sensitive to the gd-gd monopole strength in the considered nuclei.

In summary, we measured the 2^{+}_{1} and 4^{+}_{1} states in neutron-rich ^{66}Cr and ^{70,72}Fe isotopes. A plateau in the energy systematics was observed for Cr and Fe isotopes beyond N=38,40 and up to N=44,46, respectively. This plateau is interpreted within the shell model as an extension of the N=40 IoI towards more neutron-rich isotopes. While quadrupole collectivity is maximized at N=40, the evolution of pairing correlations slightly shifts the minimum of 2^{+}_{1} and 4^{+}_{1} energies to larger neutron number for both Cr and Fe isotopes. Whether this plateau extends to N=50, which would imply the disappearance of the N=50 shell closure below ^{78}Ni, requires the spectroscopy of more neutron-rich Fe and Cr isotopes. While the spectroscopy of ^{68}Cr and ^{74}Fe could be reached at SEASTAR in the near-term future with improvements of U primary beam intensity at the RIBF, the spectroscopy of more exotic isotopes should await for major upgrades or next-generation facilities.

The authors are thankful to the RIBF and BigRIPS teams for the stable operation, high intensity of the Uranium primary beam and production of secondary beams during the experiment. The development of MINOS and the core MINOS team have been supported by the European Research Council through the ERC Grant MINOS-258567. A. O. has been supported by the JSPS long-term fellowship L-13520 from Sept. 2013 to June 2014 at the RIKEN Nishina Center. A. O. deeply thanks the ERC and JSPS for their support. C. Santamaria and A. O. are grateful to the RIKEN Nishina Center for its hospitality. L.X. C. has been supported by the LIA program of Vietnam Ministry of Science and Technology (MOST). Z. D. and Zs. V. have been supported by the OTKA K100835 contract. V. W. further acknowledges support through the German BMBF grant 05P12RDFN8 and U.S. DOE under grant DE-FG02-91ER-40609. We thank N. Paul for her careful reading of the manuscript.

[1] O Sorlin and M.-G. Porquet, Prog. in Part. and Nucl. Phys. **61**, 602 (2008).
[2] E. Caurier *et al.*, Rev. Mod. Phys. **77**, 427 (2005).
[3] I. Talmi and I. Unna, Phys. Rev. Lett. **4**, 469 (1960).
[4] T. Otsuka *et al.*, Phys. Rev. Lett. **87**, 082502 (2001).
[5] T. Otsuka *et al.*, Phys. Rev. Lett. **95**, 232502 (2005).
[6] N. Smirnova *et al.*, Phys. Lett. B **686**, 109 (2010).
[7] N. Smirnova *et al.*, Phys. Rev. C **86**, 034314 (2012).
[8] E. Caurier, F. Nowacki, A. Poves, Phys. Rev. C **90**, 014302 (2014).
[9] B. H. Wildenthal and W. Chung, Phys. Rev. C **22**, 2260 (1980).
[10] A. Poves and J. Retamosa, Phys. Lett. B **184**, 311 (1987).
[11] E. K. Warburton, J. A. Becker and B. A. Brown, Phys. Rev. C **41**, 1147 (1990).
[12] T. Motobayashi *et al.*, Phys. Lett. B **346**, 9 (1995).
[13] P. Doornenbal *et al.*, Phys. Rev. Lett. **111**, 212502 (2013).
[14] J. Ljungvall *et al.*, Phys. Rev. C **81**, 061301 (2010).
[15] R. Broda *et al.*, Phys. Rev. Lett. **74**, 868 (1995).
[16] O. Sorlin *et al.*, Phys. Rev. Lett. **88**, 092501 (2002).
[17] C. Guénaut *et al.*, Phys. Rev. C **75**, 044303 (2007).
[18] S. Rahaman *et al.*, Eur. Phys. J. A **34**, 5 (2007).
[19] K. Langanke *et al.*, Phys. Rev. C **67**, 044314 (2003).
[20] M. Hannawald *et al.*, Phys. Rev. Lett. **82**, 1391 (1999).
[21] P. Adrich *et al.*, Phys. Rev. C **77**, 054306 (2008).
[22] O. Sorlin *et al.*, Eur. Phys. J. A **16**, 55 (2003).
[23] N. Aoi *et al.*, Phys. Rev. Lett. **102**, 012502 (2009).
[24] A. Gade *et al.*, Phys. Rev. C **81**, 051304(R) (2010).
[25] W. Rother *et al.*, Phys. Rev. Lett. **106**, 022502 (2011).
[26] H. L. Crawford *et al.*, Phys. Rev. Lett. **110**, 242701 (2013).
[27] S. Naimi *et al.*, Phys. Rev. C **86**, 014325 (2012).
[28] S.M. Lenzi *et al.*, Phys. Rev. C **82**, 054301 (2010).
[29] L. Gaudefroy *et al.*, Phys. Rev. C **80**, 064313 (2009).
[30] K. Sato *et al.*, Phys. Rev. C **86**, 024316 (2012).
[31] I. Hamamoto, Phys. Rev. C **85**, 064329 (2012).
[32] T. Kubo *et al.*, Prog. Theor. Exp. Phys. **2012**, 3C003 (2012).
[33] N. Fukuda *et al.*, Nucl. Instr. Meth. B **317**, 323 (2013).
[34] RIKEN Proposal for Scientific Program (2013). Acronym for Shell Evolution And Search for Two-plus states At the RIBF (SEASTAR).
[35] S. Takeuchi *et al.*, Nucl. Instr. Meth. A **763**, 596 (2014).
[36] A. Obertelli *et al.*, Eur. Phys. J. A **50**, 8 (2014).
[37] H. Kumagai *et al.*,Nucl. Instr. Meth. A **470**, 562 (2001).
[38] C. Santamaria *et al.*, to be published (2015).
[39] I. Giomataris *et al.*, Nucl. Instr. Meth. A **376**, 29 (1996).
[40] D. Calvet, IEEE Trans.Nucl. Sci., **61**, 1, 675-682 (2014).
[41] S. Anvar et al., Proc. IEEE Nuclear Science Symp., pp. 745-749 (2011).
[42] S. Agostinelli *et al.*, Nucl. Instr. Meth. A **506**, 250 (2003).
[43] S.N. Liddick *et al.*, Phys. Rev. C **87**, 014325 (2013).

[44] F. Recchia *et al.*, Phys. Rev. C **88**, 041302(R) (2013).
[45] A. Gade *et al.*, Phys. Rev. Lett. **112**, 112503 (2014).
[46] F. Flavigny *et al.*, Phys. Rev. C **91**, 034310 (2015).